Jurnal Polimesin
Department of Mechanical Engineering
State Polytechnic of Lhokseumawe
http://e-jurnal.pnl.ac.id/polimesin
e-ISSN : 2549-1999 No. : 6 Month : December
p-ISSN : 1693-5462 Volume : 23 Year : 2025

Processing dates: received on 2025-09-30, reviewed on 2025-11-07, accepted on 2025-12-15 and online availability on 2025-12-31

Effect of water pressure and temperature on the performance of a desalination reactor

Dany Alvian Dwibowo[1], Dan Mugisidi[1*], Oktarina Heriyani[1], Rizky Alamsyach[1], Syahrul Amin[1]
[1] Department of Mechanical Engineering, Muhammadiyah Prof. Dr. Hamka University, Jakarta 13830, Indonesia
*Corresponding author: dan.mugisidi@uhamka.ac.id

Abstract

The crisis of clean water availability has become increasingly critical due to rapid population growth and environmental degradation. One strategic approach to address this challenge is to implement seawater desalination, which provides an abundant, sustainable water source. However, conventional methods remain limited in terms of energy efficiency. This study aims to analyze the effect of pressure and temperature variations on the performance of a large-capacity desalination reactor with an 8000-liter tank. Two configurations were experimentally tested: (1) an air-circulation system that relies on static heating assisted by an axial fan to enhance convection, and (2) a sealed system operating under low-pressure conditions to reduce the boiling point of water, equipped with active hot-water circulation. Data collection was carried out over 27 hours of operation, with the observed parameters including water temperature, partial pressure, relative humidity, and evaporation volume. The experimental results showed that the sealed configuration delivered superior performance, with an evaporation rate 16.64% higher than that of the air-circulation variant. The volume of water successfully evaporated in the sealed system reached 20.12 liters, whereas in the air-circulation system it was only 17.25 liters. This increase in efficiency is attributed to the pressure-reduction effect, which enhances the vapor pressure difference while facilitating uniform heat distribution through active water circulation. This study emphasizes that controlling pressure and temperature is key to improving the effectiveness of the desalination process, thereby supporting the Development of more energy-efficient and sustainable clean water supply technologies.

Keywords:
Desalination reactor, water evaporation, vacuum pressure, thermal performance, freshwater production

1 Introduction

Water is an essential component that supports human life and other living organisms [1]. Although about 71% of the Earth's surface is covered by water, the majority is seawater (approximately 97%), while freshwater accounts for only about 3%. Of this amount, only about 0.06% of freshwater is directly available for human needs, and its availability is unevenly distributed across different regions of the world [2]. Unfortunately, the availability of clean water worldwide continues to decline [3]. Several factors cause this phenomenon, including pollution, the impacts of climate change, and population growth[4]. According to a WHO report, around 2.1 billion people worldwide still lack access to safe drinking water [5].

To meet the demand for clean water, seawater can be desalinated [6]. According to the latest report from the International Desalination Association (IDA), by the end of 2022, 22,757 desalination facilities were operating worldwide, with a combined production capacity of approximately 107.95 million cubic meters per day [7]. In other words, these data indicate the rapid growth of desalination technology to address the limitations of global freshwater resources.

Desalination is the process of separating dissolved salts from seawater to obtain freshwater that meets utilization standards through the evaporation phase [8]. The vapor is then cooled until it condenses into pure water droplets or distillate water (freshwater) [9]. Several desalination methods have been developed, including distillation, Reverse Osmosis (RO), and electrodialysis [10]. Among these methods, desalination reactors based on thermal and pressure principles are considered effective for fornhancing the separation of water from salt [11]. In global practice, the most widely applied desalination methods include RO, Multi-Effect Distillation (MED), and Multi-Stage Flash Distillation (MSF), each with distinctive operational characteristics and significant dependence on process factors, particularly pressure and temperature [8][12].

Pressure and temperature are the main operating parameters that significantly influence the evaporation rate and performance efficiency of desalination systems that utilize thermal energy [13]. In the evaporation process, increasing the water temperature increases the molecules' kinetic energy, thereby accelerating the phase change from liquid to vapor [14]. In addition, low pressure lowers the boiling point of water, allowing evaporation to occur more rapidly with lower energy requirements [15]. The airflow over the liquid surface serves as a carrier for the vapor formed by evaporation[16]. The acceleration of airflow enhances mass transfer by reducing relative humidity near the surface, thereby helpingaintain the stability of the vapor concentration gradient [17]. This is explained in a study by Omar dkk [18, which demonstrated that applying a hot-air circulation configuration can increase the evaporation rate by 16–20% compared to conditions without active airflow.

A previous study by Irham et al. [19]found that using an air pump to induce convective flow, combined with seawater heating, directly accelerates evaporation. The thermal energy supplied is absorbed by the water in the heating system, causing vapor to form and flow into the condenser. With an air pump, evaporation efficiency increases due to higher air pressure and movement, which accelerate evaporation and condensation, thereby producing a larger volume of freshwater than traditional methods. Subsequently, a study by Alamsyach et al. [20] revealed that combining increased airflow velocity with simultaneous water heating effectively enhanced the evaporation rate and the yield of clean water. The system utilizes solar thermal energy and actively controlled airflow, enabling them to work together to achieve higher efficiency.

Furthermore, a study by Ghazouani et al. [21] also explained that the performance of desalination systems is strongly influenced by operating parameters, including cycle configuration, the heating method employed, and the air circulation mechanism. The increase in fluid temperature, both water and air, has been proven to accelerate the evaporation rate, although on the other hand, it results in higher energy requirements. The system used in this study is conventional humidification–dehumidification desalination, in which the process still relies on natural flow, resulting in only limited heat and mass transfer coefficients. This means that forced convection, achieved with fans or air pumps, is more effective at accelerating evaporation and condensation, thereby improving system productivity.

To date, research specifically examining the effects of water pressure and temperature in desalination reactors equipped with large-capacity tanks remains very limited. Most previous studies have been conducted on small-scale systems that cannot accurately represent evaporation performance or the process stability required for large-scale desalination operations. This research is necessary because the global and national clean water crisis continues to worsen, while demand for freshwater is increasing [22].

At the same time, Indonesia still relies on industrial salt imports due to the low purity of locally produced salt and its limited

production volume [23]. Large-capacity thermal desalination systems have the potential to address both issues simultaneously by producing clean water while also generating high-quality salt as a valuable by-product. Therefore, this study aims to evaluate the effects of water pressure and temperature on the evaporation rate in a large-capacity desalination reactor and to determine the most effective operating conditions for enhancing desalination process performance

2 Research methodology

This study investigates the performance of an 8000 L tank used as a desalination unit in two variants: the Air Circulation Variant and the Airtight Variant. In the air circulation variant, the water is heated (≥50˚C), the hot water circulation pump is turned off, the centrifugal blower is open, the air heater is turned off, and the axial fan is turned on. Under non-vacuum conditions, the boiling point of water remains higher, so the evaporation process occurs at ≥50°C without a reduction in boiling point due to low pressure. Without circulation pump flow, the heat in the water does not distribute evenly, leaving the upper partarmer while the lower part remains cooler [24]. Meanwhile, the airflow generated by the axial fan and the open centrifugal blower creates circulation above the water surface and around the tank, thereby helping to carry the vapor produced by evaporation. In the airtight variant, the water temperature is set the same as in the air circulation variant (≥50°C), the hot water circulation pump is turned on, the centrifugal blower is closed, the air heater is turned off, and the axial fan is turned on. When the air inlet is closed, and the axial fan operates, a partial vacuum is created inside the tank, lowering the boiling point of water and enabling more efficient evaporation at lower temperatures [25]. The circulation pump helps equalize heat distribution, while the airflow from the axial fan maintains the vapor concentration gradient at the water surface, thereby increasing the evaporation rate even without an air heater [26]. The research variables are shown in Fig. 1.

(a) (b)

Fig. 1. Centrifugal blower. a) Air circulation, and b) Airtight

The data collection process begins with measurements from the Level Glass, T_1, T_2, T_3, T_5, and T_6, followed by RH_1, RH_2, and RH_3, which are recorded sequentially. To measure the vacuum pressure generated by the axial fan's airflow, a PCE pressure meter was used [27]. The level glass was used to measure the water mass in the tank and determine the mass reduction due to evaporation. The water in the main tank was heated by a water heater and circulated by a water pump to maintain a temperature between 50°C and 55°C. Data were collected every 1 hour during each experimental session, which lasted 9 hours. For each variant, the experiments were conducted on three separate days, yielding three independent replicates. The experiment was carried out at the Mechanical Engineering Laboratory, Faculty of Industrial Technology and Informatics, Universitas Muhammadiyah Prof. Dr. Hamka. The experimental setup used in this study is presented in Fig. 2, with the specifications shown in Table 1. The measuring instruments employed are listed in Table 2.

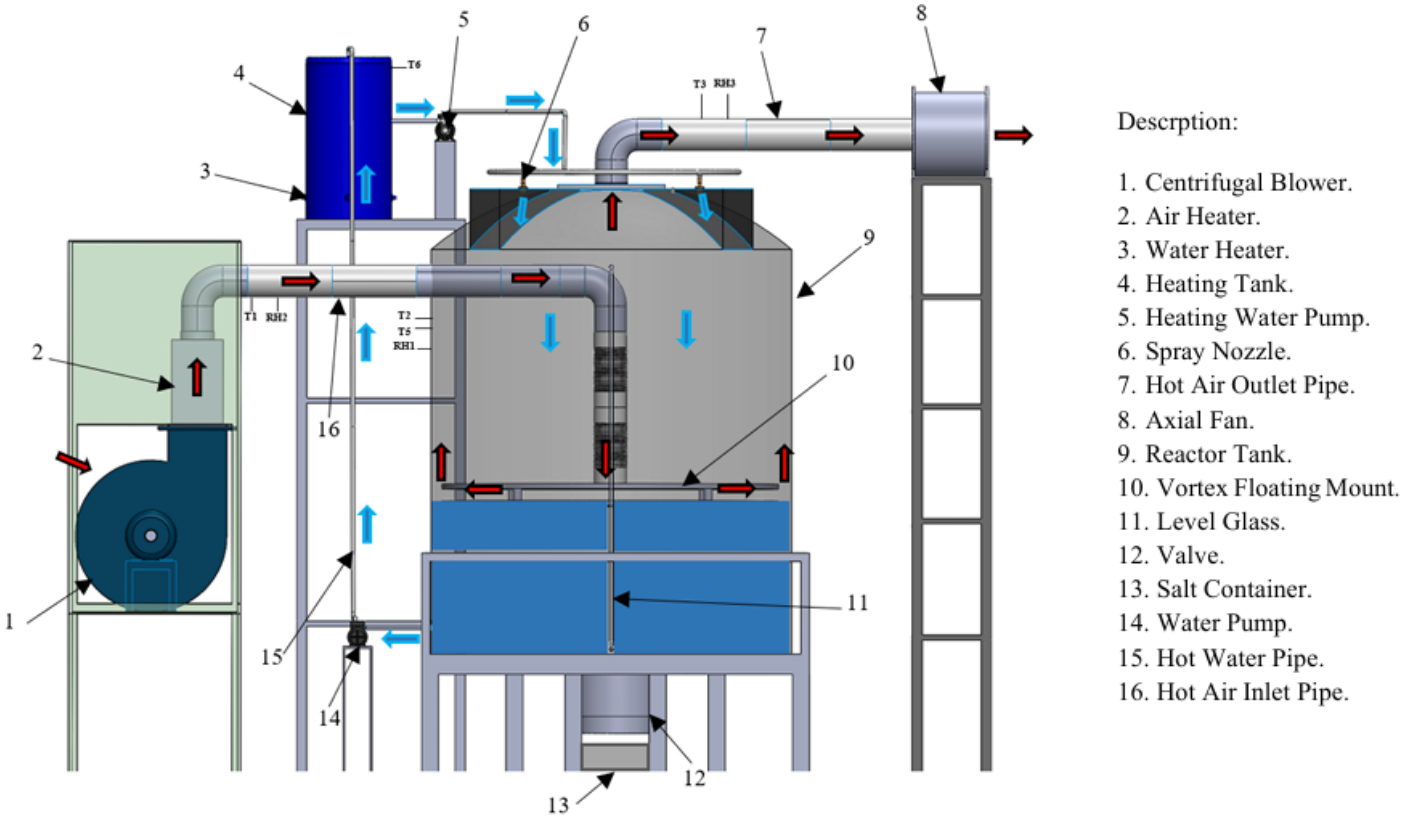

Fig. 2. Schematic framework of the desalination reactor research

In this research, a centrifugal cover with a U-tube manometer is used to compare its performance as a desalination device. This study employs an experimental method in which 3472 liters or 1085 mm of fresh water is placed into the tank, then equipped with a vortex generator that functions to produce a swirling airflow (vorticity) and enhance the turbulence level on the water surface, thereby accelerating the evaporation rate [28]. The vortex generator is placed beneath the floating vortex holder, directly facing the water surface. The water is circulated using a water pump from inside the tank. To increase the water temperature, a heating tank is used. The heating

tank is equipped with four heaters to maximize heat, and is further assisted by direct solar heating.

Table 1. Desalination reactor unit specifications

Unit	Spesification
Centrifugal blower	16", 4000 W, 1450 RPM
Air heater	5 pcs, 1000 W
Water heater	4 pcs, 1000 W
Heating tank	150 L, diameter 510 mm, high 1020 mm
Water pump	27 m, 18 L/min
Spray nozzle	4 pcs, 6 – 12 m, 1/2"
Hot air outlet and inlet pipe	8"
Axial fan	0.75 kW, 1400 RPM
Reactor tank	8000 L, diameter 2140, high 2500 mm
Vortex floating mount	diameter 2040 mm
Hot water pipe	1/2"

Table 2. Measurement tools

Tools	Function	Spesification
Digital thermometer (T_1 – T_6)	Temperature	-50°C - 110°C, ±0.1°C
Digital hygrometer (RH_1 – RH_3)	Humidity	10% - 99%, ±1°C
Anemometer (v)	Wind velocity	0 – 30 m/s, Resolution 0.1 m/s
Pressure meter PCE (P)	Pressure	¼ inch, 12 mm
Level glass (mm)	Water level	½ inch, high 2100 mm

Then, the hot water from the heating tank is fed back into the top of the reactor through a spray nozzle at medium pressure. The water temperature ranges from 50°C to 60°C. The centrifugal blower draws air through the blower inlet and passes it through the air heater. Then, the air enters through the air pipe toward the bottom of the vortex holder, subsequently flowing between the vortex holder and the water. The air will contact the vortex, creating vorticity and evaporating the water. The distance between the vortex holder and the water surface is 70 mm. The airflow temperature ranges from 65°C to 70°C. The velocity of the incoming airflow into the reactor tank is 6.3 m/s. The water level decreases, and the floating vortex holder descends following the water surface. When seawater is used, the salt crystals that settle at the bottom of the reactor tank can be collected and transferred to the salt reservoir via a valve at the reactor bottom. An axial fan draws out the water vapor inside the tank.

The overall result of the desalination reactor assembly (Fig. 3 andFig. 4), which integrates various aspects of technical design and construction, can be seen in Fig. 5.

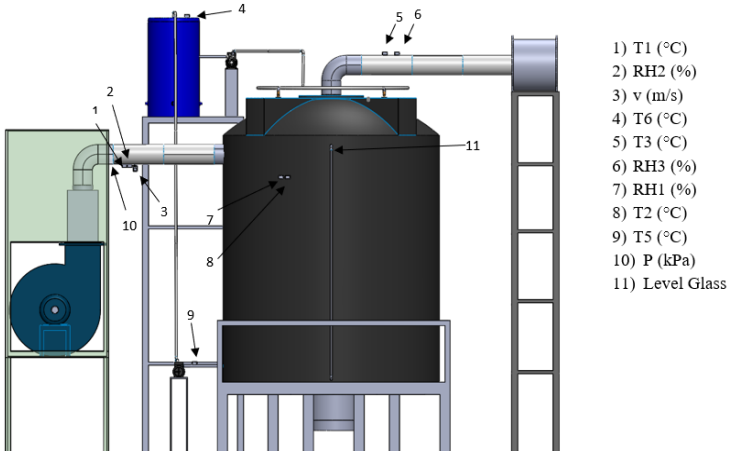

Fig. 3. Position of the measuring instruments from the right-side view

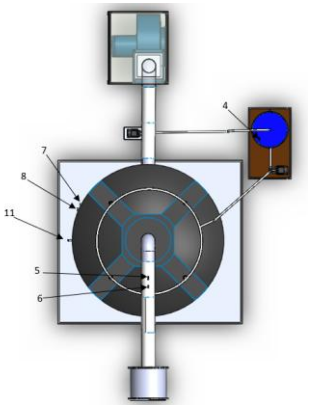

Fig. 4. Position of the measuring instruments from the top view

Fig. 5. Desalination reactor construction

To quantify the dispersion of the measurement results relative to the mean, the standard deviation was used (Eq. (1)).

$$s = \sqrt{\frac{\sum_{i=1}^{n}(x_i - \bar{x})^2}{n-1}} \quad (1)$$

where x_i is represents the evaporation value at the *i*-th run, $\bar{x}$ is denotes the mean value of the three runs, and n is the number of independent runs [29]. The experimental uncertainty can be obtained from Eq. (2).

$$\sigma = \sqrt{\frac{\sum(P_i - \bar{P})^2}{N}} \quad (2)$$

where P_i is the *i*-th value of the observed variable, $\bar{P}$ is the population mean, and N is the total number of experimental data points [30]. Because the reactor tank is cylindrical, the cross-sectional area can be obtained from Eq. (3).

$$A = \frac{\pi D^2}{4} \quad (3)$$

where A is the cross-sectional area of the reactor (m^2), π is the mathematical constant (3.14 or 22/7), and D is the tank diameter (mm) [31]. The change in fluid height within the reactor is calculated from the geometric relationship between the change in volume and the reactor's cross-sectional area. The change in fluid surface height (Δh) is determined using Eq. (4).

$$\Delta h = \frac{V}{A} \quad (4)$$

where Δh is the decrease in water surface height (mm), V is the volume of evaporated water (L), and A is the cross-sectional area of the reactor (m²) [32]. To calculate the power value in an electrical circuit, Eq. (5) is used.

$$P = V \times I \quad (5)$$

where P is electrical power (Watt), V is supplied voltage (Volt), and I is electric current (Ampere) [33]. As time progresses, the magnitude of electrical power in a circuit can be expressed through Eq. (6).

$$W = \frac{P \times t}{1000} \quad (6)$$

where W is electrical energy (kWh), P is electrical power (W), and t is time unit (hours) [33].

3 Results and discussion

The presence of a closed, low-pressure system space and active hot water circulation influences the effectiveness of the airtight variant. The pressure reduction inside the system creates semi-vacuum conditions that lower the boiling point of water, allowing evaporation to occur more rapidly even when the temperature is maintained above 50°C. In addition, the circulation of the hot-water pump accelerates the distribution of thermal energy throughout the liquid volume, thereby maximizing heat and mass transfer. The effectiveness of the system is highly dependent on the rate of evaporation[34]. The higher the evaporation rate, the greater the system's thermal efficiency, as more heat energy is directly absorbed to convert water into vapor rather than being lost to the environment [35][36].

In the Air Circulation Variant, the water is heated to a minimum temperature of 50°C without an active circulation pump. This means that heating occurs only statically. The axial fan is operated while the centrifugal blower remains inactive and open, thereby preventing the formation of negative pressure. Under these conditions, the air flows freely into or out of the system without restriction. Since there is no active circulation of the heating water, the generated heat accumulates in certain areas, resulting in temperature stratification and ultimately a non-uniform heat distribution. The axial fan provides only limited airflow and lacks sufficient capacity to enhance heat convection effectively [37] [38]. The system functions passively and cannot sustain stable and uniform temperature conditions [39].

As shown in Fig. 6. Evaporation results of the air circulation variant and the airtight variant, the airtight variant demonstrates a higher evaporation rate compared to the air circulation variant. During the 27-hour observation period, the volume of water evaporated by the Airtight Variant reached 20.12 L, while the Air Circulation Variant achieved only 17.25 L.

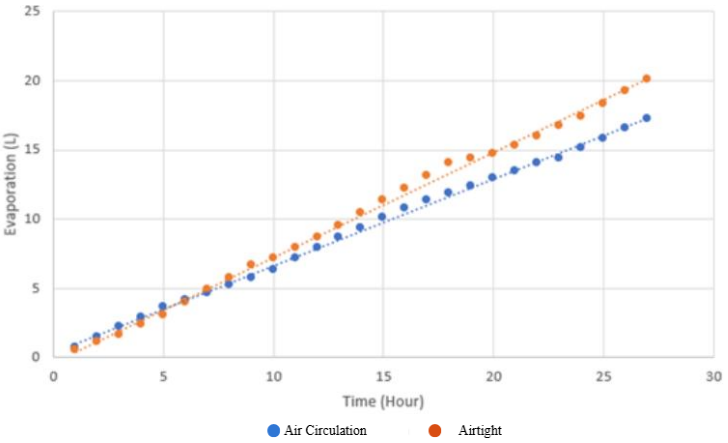

Fig. 6. Evaporation results of the air circulation variant and the airtight variant

In other words, the evaporation rate of the airtight variant was 16.64% higher than that of the air circulation variant. these results indicate that the system configuration applied to the two variants significantly affects the acceleration of the liquid-to-vapor phase transition. In the airtight variant, the lower pressure combined with a higher water temperature increases the pressure difference between the water and the space above it. This is consistent with the findings of [40], which reported that the efficiency of the evaporation process in air-cooled desalination systems increases significantly when the fluid temperature is raised, and the air pressure above the surface is reduced, particularly when airflow velocity is increased in a controlled manner. Eq. (7) is used to calculate the saturated vapor pressure of water at a given temperature.

$$P_w = exp\left[25.317 - \frac{5144}{T_w + 273}\right] \quad (7)$$

where P_w is water pressure (Pa), T_w is water Temperature (°C) [41]. Eq. (8) is applied to determine the vapor mass flow rate generated by the pressure differential.

$$m = \frac{\Delta P}{h_{fg}} \quad (8)$$

where ṁ is mass flow rate (kg/s), ΔP is pressure differential (Pa), h_{fg} is latent heat of vaporization (kJ/kg) [42].

The sensitivity analysis indicates that (Fig. 7), within the range of mass transfer coefficients (k_g) obtained under forced convection conditions (10^{-3} to 10^{-2} m s^{-1}), the mass flux per unit area, determined using 2.07×10^{-5} to 2.07×10^{-4} kg.$m^{-2}s^{-1}$. This corresponds to an evaporation rate of about 1.79 L m-2 day^{-1}. From a theoretical perspective, if the system configuration can increase the mass transfer coefficient to approximately 10^{-2} m^{-2} s^{-1}, the predicted values per unit area would align with the experimental results [43].

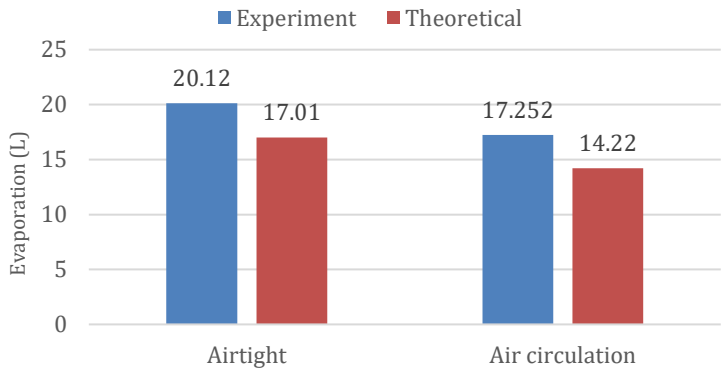

Fig. 7. Comparison of experimental and theoretical results (air circulation and airtight variants)

The evaporation process was analyzed using the principles of thermodynamics and classical mass-transfer mechanisms. The saturated water vapor pressure as a function of temperature is

expressed using the Antoine equation, Log_{10} P = A - $\frac{B}{C+T}$ (constans A,B, C) (chosen according to the temperature range used) or, for estimating changes in vapor pressure between conditions, the Clausius–Clapeyron equation in integrated form with $\ln\frac{p_{s,2}}{p_{s,1}} = -\frac{h_{fg}}{R_v}\left(\frac{1}{T_2}-\frac{1}{T_1}\right)$ with $R_v = \frac{R}{M_w}$ The vapor mass flux is expressed directly in terms of the partial pressure difference between the surface and the headspace as $J = h_m\,(p_s - p_w)$ (kg/m^{-2}s^{-1}). Where p_s and p_w are the saturated vapor pressure at the surface temperature and the partial vapor pressure in air (Pa), h_m is the mass transfer coefficient in units of $kg.m^{-2}.s^{-1}.Pa^{-1}$, and the total mass rate $\dot{m} = J.A$. The theoretical estimation of hm can be obtained from dimensional correlations. First, the Sherwood number is calculated $Sh_L = \frac{k_c L}{D_{v,a}}$ using the forced convection correlation over a flat plate. However, for practical accuracy in this study, experimental measurements were used and calculated theoretically by measuring the mass reduction $\Delta m/\Delta t$ to obtain $J_{exp} = \frac{\dot{m}_{exp}}{A}$ and then calculating $h_m = \frac{J_{exp}}{(p_s - p_w)}$.

In applying the evaporation model to this desalination reactor, several operating assumptions were established to ensure that the theoretical calculations are consistent with the experimental field conditions. The evaporation process is assumed to be in quasi-steady state during the measurement period, as data were recorded hourly and the system did not experience significant changes in heating patterns or airflow. The water-surface temperature is treated as uniform, particularly in the airtight variant equipped with active circulation, so that heat distribution is considered homogeneous and the saturated vapor pressure (psp_sps) can be determined from a single surface temperature. Conduction losses within the fluid and heat losses to the environment are not included in the model, as the analytical focus of this document is on vapor pressure differences and circulation effects rather than a detailed energy balance. The airflow from the axial fan is assumed to form a thin boundary layer above the water surface, such that empirical equations, including those relating wind speed, vapor pressure difference, and evaporation rate, remain valid for the tested air circulation and airtight configurations. The air–water vapor mixture in the headspace is treated using directly measured partial pressures and relative humidity.

The Airtight Variant: the combination of liquid circulation maintains the surface temperature, the axial fan thins the vapor boundary layer and increases the mass transfer coefficient, and the blower, in a closed or vacuum condition, reduces the partial pressure of water vapor, thereby enlarging the pressure difference. Consequently, both the mass transfer coefficient and the pressure difference increase, resulting in a higher actual flux [44]. Accordingly, the experimental result of the Airtight Variant (≈20.12 L over 27 hours) surpasses the theoretical prediction (≈17.25 L), corresponding to a deviation of 15.5%.

Partial vacuum in this system is achieved by evacuating air from a closed chamber until the internal pressure falls below atmospheric pressure. Fig. 8 to Fig. 11 present the absolute and gauge pressures as functions of time, along with their associated uncertainties. Based on the previous calculations, the experimental pressure uncertainty was obtained as σ = 0.0117355403 kPa for the air circulation variant and σ = 14.97667 kPa for the airtight variant.

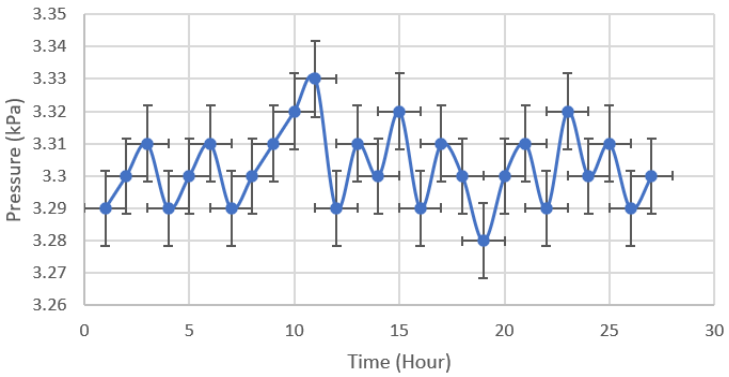

Fig. 8. Absolute pressure varies air circulation

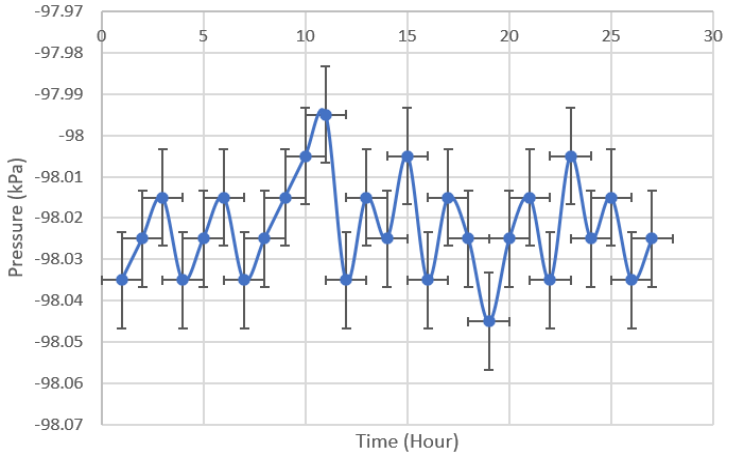

Fig. 9. Gauge pressure varies air circulation

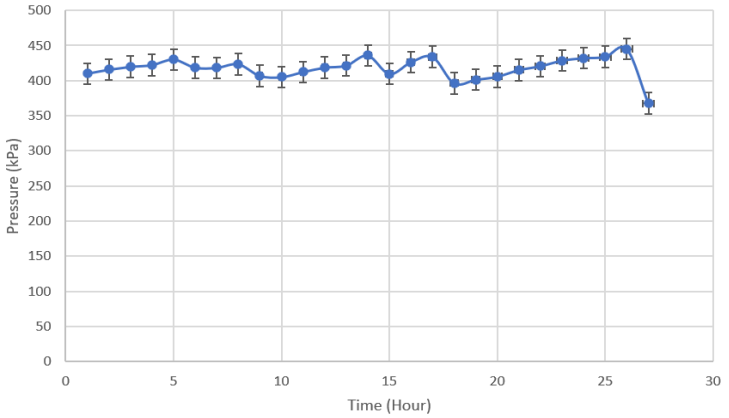

Fig. 10. Absolute pressure varian airtight

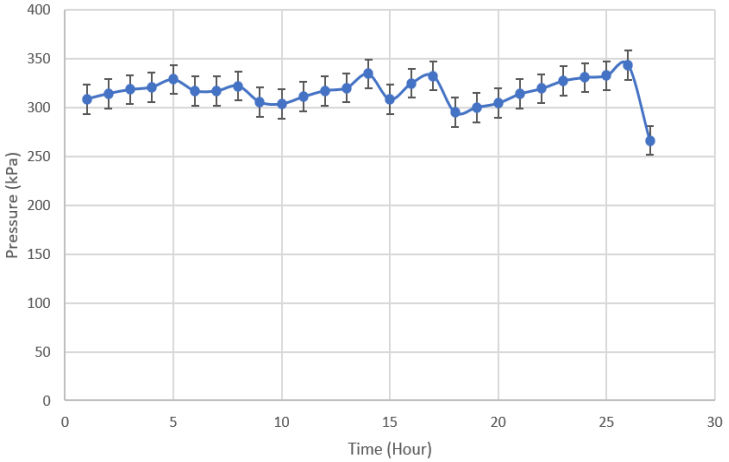

Fig. 11. Gauge pressure varies airtight

A reduction in the number of gas molecules within the system results in a decrease in absolute pressure, as reflected by negative gauge pressure values. The establishment of this condition is further supported by water circulation, which facilitates the removal of trapped air, reduces dead volume, and helps maintain pressure and temperature stability during the process. As the amount of free air

decreases, the system reaches an equilibrium state in which the air-evacuation rate equals the micro-leakage rate

Once a partial vacuum is established, pressure stability is maintained through an airtight system. All components and connections are designed to be airtight to limit air ingress from the surrounding environment. This condition is evidenced by relatively stable absolute and gauge pressures over time, with minor fluctuations that remain within the measurement uncertainty limits. These fluctuations are attributable to water flow dynamics, temperature variations, and instrument response, without indicating any significant degradation in vacuum quality.

Based on measurements conducted over three days at nine time points per day, the mean values and standard deviations of the measured parameters were obtained, as presented in Table 3. The temperature parameters exhibited good stability, with values of T_1: 40.53 ± 1.08°C, T_2: 52.52 ± 1.52°C, T_3: 52.36 ± 1.50°C, T_5: 55.16 ± 2.19°C, and T_6: 36.81 ± 2.28°C. The relatively low standard deviation values indicate minimal temperature fluctuations.

Relative humidity also remained stable, with average values of RH_1: 76.26 ± 1.85%, RH_2: 12.59 ± 5.01%, and RH_3: 90.33 ± 1.86%. The most significant variation was observed in RH_3, indicating higher humidity dynamics at that measurement point. The operating pressure was consistently recorded at 3.30 ± 0.01 kPa, while the airflow velocity remained constant at 6.3 ± 0 m/s, in accordance with the setpoint. The glass level parameter was 1082.963 ± 1.315 mm, with only very minor changes observed during the operational process, as shown in Table 3.

Table 3. Mean values and standard deviations of the air circulation variant

Parameter	Mean	Standar Deviation (SD)	Mean ± SD
T_1 (°C)	40.53	1.08	40.53 ± 1.08
T_2 (°C)	52.52	1.52	52.52 ± 1.52
T_3 (°C)	52.36	1.50	52.36 ± 1.50
T_5 (°C)	55.16	2.19	55.16 ± 2.19
T_6 (°C)	36.81	2.28	36.81 ± 2.28
RH_1 (%)	76.26	1.85	76.26 ± 1.85
RH_2 (%)	12.59	5.01	12.59 ± 5.01
RH_3 (%)	90.33	1.86	90.33 ± 1.86
P (kPa)	3.30	0.01	3.30 ± 0.01
Evaporation volume (L)	0.639	0.087	0.639 ± 0.087
V (m/s)	6.3	0	6.3 ± 0
Level glass (mm)	1082.963	1.315	1082.963 ± 1.315

The mean and standard deviation for each observed parameter were determined from 27 data points. The analysis results indicate that the temperatures at points T_1–T_6 were within the ranges of 43.33 ± 0.07 °C, 54.88 ± 0.13 °C, 54.54 ± 0.18 °C, 55.07 ± 0.27 °C, and 60.25 ± 0.12 °C. The relative humidity values at RH_1, RH_2, and RH_3 were 83.33 ± 2.04%, 35.11 ± 5.76%, and 94.89 ± 1.01%, respectively. The operating pressure was 417.87 ± 15.42 kPa, while the evaporated volume rate was 0.67 ± 0.63 L. The air velocity (v) remained stable at 6.30 ± 0.00 m/s, and the glass level was recorded at 1081.89 ± 1.99 mm, as shown in Table 4.

Table 4. Mean values and standard deviations of the airtight variant

Parameter	Mean	SD	Mean ± SD
T_1 (°C)	43.33	0.07	43.33 ± 0.07
T_2 (°C)	54.88	0.13	54.88 ± 0.13
T_3 (°C)	54.54	0.18	54.54 ± 0.18
T_5 (°C)	55.07	0.27	55.07 ± 0.27
T_6 (°C)	60.25	0.12	60.25 ± 0.12
RH_1 (%)	83.33	02.04	83.33 ± 2.04
RH_2 (%)	35.11	5.76	35.11 ± 5.76
RH_3 (%)	94.89	01.01	94.89 ± 1.01
P (kPa)	417.87	15.42	417.87 ± 15.42
Evaporation volume (L)	0.67	0.63	0.67 ± 0.17
V (m/s)	6.30	~0	6.30 ± 0.00
Level glass (mm)	1081.89	1.99	1081.89 ± 1.99

To evaluate the statistical significance of the 16.64% increase in volume, a Mann–Whitney U test was conducted as the nonparametric counterpart of the two-sample *t*-test (Fig. 12). This test compared the performance of two system configurations, namely air circulation and airtight, each based on 27 independent observations (Table 5 and Table 6). The analysis results showed that the Airtight configuration had a higher mean rank (35.02) than the Air Circulation configuration (19.98), indicating a more systematic distribution of volume. The statistical test yielded U = 161.50, Z = −3.513, with $p < 0.001$ (two-tailed), confirming a statistically significant difference between the two configurations. Therefore, the 16.64% increase in volume observed for the airtight configuration is statistically significant and not attributable to random variation. These findings provide strong quantitative evidence that modifying the system to an airtight condition substantially improves volumetric performance relative to the air-circulation configuration.

Mann-Whitney Test

Ranks

	Variant	N	Mean Rank	Sum of Ranks
Volume	Air Circulation	27	19.98	539.50
	Airtight	27	35.02	945.50
	Total	54		

Test Statistics[a]

	Volume
Mann-Whitney U	161.500
Wilcoxon W	539.500
Z	-3.513
Asymp. Sig. (2-tailed)	<.001

a. Grouping Variable: Variant

Fig. 12. Mann–Whitney U test of the two variants

Table 5. Independent run data for the air circulation variant

Day	Time (WIB)	T1 (°C)	T2 (°C)	T3 (°C)	T5 (°C)	T6 (°C)	RH1 (%)	RH2 (%)	RH3 (%)	P (kPa)	Evaporation Volume (L)	v (m/s)	LEVEL GLASS (mm)	
First	9:00	42.6	54.5	54.3	57.6	40.1	77	27	91	3.29	0.50	6.3	1085	
	10:00	41.9	53.8	53.7	56.8	39.2	75	15	90	3.3	0.23	6.3	1085	
	11:00	41.4	53	53	55.9	37.9	76	10	91	3.31	0.56	6.3	1085	
	12:00	41	52.7	52.5	55.5	36.8	75	10	90	3.29	0.63	6.3	1085	
	13:00	40.6	51.9	51.6	54.9	35.9	75	10	90	3.3	0.52	6.3	1084	
	14:00	40.1	51.4	51.1	54.5	35.1	74	10	88	3.31	0.61	6.3	1084	
	15:00	39.7	50.8	50.5	53.8	34.2	74	10	88	3.29	0.49	6.3	1084	
	16:00	39.4	50.3	50.1	53.2	33.4	73	10	87	3.3	0.61	6.3	1084	
	17:00	39	49.5	49.9	52.7	32.6	73	10	86	3.31	0.68	6.3	1084	
Second	9:00	42.7	54.9	54.7	59.5	40.2	79	23	94	3.32	0.38	6.3	1084	
	10:00	42	54.5	54.2	58.5	39.4	79	17	93	3.33	0.51	6.3	1083	
	11:00	41.8	53.7	53.8	57.5	38.7	78	15	90	3.29	0.42	6.3	1083	
	12:00	41.3	53.4	53.1	56.5	37.9	75	10	92	3.31	0.49	6.3	1083	
	13:00	40.7	52.6	52.6	55.5	37.3	77	10	91	3.3	0.33	6.3	1083	
	14:00	40.1	52.1	52.1	54.5	36.8	77	10	89	3.32	0.46	6.3	1083	
	15:00	39.9	51.7	51.6	53.5	35.4	76	10	90	3.29	0.59	6.3	1082	
	16:00	39.4	51.1	51	52.5	34.7	76	10	90	3.31	0.34	6.3	1082	
	17:00	39.2	50.8	50.5	51.5	33.8	74	10	89	3.3	0.65	6.3	1082	
Third	9:00	41.4	54.9	54.7	58.2	40	78	24	93	3.28	0.52	6.3	1082	
	10:00	41.1	54.6	54.4	57.4	39.6	79	19	93	3.3	0.62	6.3	1082	
	11:00	40.9	53.8	53.6	56.7	38.9	79	10	90	3.31	0.47	6.3	1082	
	12:00	40.3	53.3	53.1	55.9	37.8	78	10	92	3.29	0.64	6.3	1082	
	13:00	39.9	52.8	52.6	55.1	37.2	75	10	91	3.32	0.53	6.3	1081	
	14:00	39.7	52.2	52	54.3	36.9	78	10	90	3.3	0.58	6.3	1081	
	15:00	39.6	51.7	51.4	53.5	35.5	76	10	91	3.31	0.61	6.3	1081	
	16:00	39.5	51.4	51.1	52.7	34.8	77	10	90	3.29	0.54	6.3	1081	
	17:00	39.2	50.7	50.4	51.2	33.7	76	10	89	3.3	0.74	6.3	1081	

Table 6. Independent run data for the airtight variant

Day	WAKTU (WIB)	T1 (°C)	T2 (°C)	T3 (°C)	T5 (°C)	T6 (°C)	RH1 (%)	RH2 (%)	RH3 (%)	P (kPa)	Evaporation Volume (L)	v (m/s)	LEVEL GLASS (mm)	
First	9:00	43.4	54.8	54.3	54.7	60	80	30	93	410.12	0.82	6.3	1085	
	10:00	43.4	54.8	54.3	54.8	60.1	80	32	95	415.77	0.71	6.3	1085	
	11:00	43.4	54.9	54.3	54.9	60.2	82	32	95	419.85	0.69	6.3	1085	
	12:00	43.3	54.9	54.4	55	60.2	81	28	94	422.93	0.76	6.3	1084	
	13:00	43.3	54.9	54.4	55	60.3	81	26	93	430.24	0.73	6.3	1084	
	14:00	43.4	54.9	54.4	55.1	60.3	83	29	94	413.66	0.71	6.3	1084	
	15:00	43.4	54.9	54.4	55.2	60.4	84	24	94	418.44	0.76	6.3	1084	
	16:00	43.3	54.9	54.4	55.3	60.3	86	26	96	423.51	0.68	6.3	1083	
	17:00	43.3	54.9	54.4	55	60.4	86	26	96	406.95	0.85	6.3	1083	
Second	9:00	43.2	54.9	54.5	54.5	60	81	45	94	405.12	0.51	6.3	1083	
	10:00	43.2	54.9	54.7	54.6	60.1	82	41	95	412.37	0.57	6.3	1083	
	11:00	43.3	54.9	54.6	54.8	60.2	82	42	95	418.66	0.64	6.3	1082	
	12:00	43.3	55	54.8	55	60.2	82	38	95	421.55	0.72	6.3	1082	
	13:00	43.3	55	54.7	55	60.3	83	38	95	435.88	0.84	6.3	1082	
	14:00	43.4	55	54.8	55.1	60.3	85	36	94	409.74	0.66	6.3	1082	
	15:00	43.4	55.1	54.9	55.2	60.3	85	36	96	426.31	1.03	6.3	1081	
	16:00	43.3	55.1	54.9	55.4	60.4	86	36	96	433.92	0.98	6.3	1081	
	17:00	43.4	55.1	54.8	55.4	60.4	86	37	97	396.92	1.22	6.3	1081	
Third	9:00	43.2	54.6	54.4	54.8	60.1	81	44	94	401.45	1.03	6.3	1081	
	10:00	43.3	54.6	54.4	55	60.1	83	39	94	409.82	1.49	6.3	1080	
	11:00	43.3	54.7	54.5	55.1	60.2	82	41	95	415.29	0.11	6.3	1080	
	12:00	43.4	54.7	54.4	55.2	60.2	84	38	95	420.73	0.18	6.3	1080	
	13:00	43.3	54.9	54.5	55.2	60.3	83	38	95	428.66	0.32	6.3	1080	
	14:00	43.4	54.8	54.5	55.3	60.3	85	36	94	432.18	0.36	6.3	1079	
	15:00	43.4	54.8	54.6	55.4	60.3	85	37	96	439.57	0.54	6.3	1079	
	16:00	43.3	54.8	54.6	55.5	60.4	86	36	96	445.11	1.59	6.3	1079	
	17:00	43.4	54.9	54.6	55.5	60.4	86	37	96	367.66	0.62	6.3	1079	

In the air circulation variant, the saturated vapor pressure of water is calculated using Eq. (9).

$$\log_{10} P = A - \frac{B}{C + T} \tag{9}$$

where A, B, C are specific constants of water, T is water temperature (°C) [45]. Eq. (10) is then used to calculate the evaporation rate.

$$El_p = (0.37 + 0.0041\bar{u})(p_s - p_w)^{0.88} \quad (10)$$

Where El_p is the evaporation rate (L/day), $\bar{u}$ is wind speed (m/s), p_s is saturated water vapor (kPa), and p_w is actual water vapor in the atmosphere (kPa) [46].

Experimental observations of the air circulation variant (Fig. 13) show that the water evaporation rate is approximately 5.75 L per day, for a total of 17.252 L over three days. In contrast, the theoretical estimate is only 4.74 L per day, for a total of 14.22 L over three days (Fig. 14). The approximately 21% difference indicates that evaporation does not depend solely on the vapor pressure difference but is also influenced by solar radiation and the airflow pattern around the water surface [47][48].

Day	Time (Hour)	LEVEL GLASS (mm)
First	1	1084.9
	2	1084.8
	3	1084.6
	4	1084.5
	5	1084.3
	6	1084.2
	7	1084.0
	8	1083.8
	9	1083.7
Second	10	1083.6
	11	1083.4
	12	1083.3
	13	1083.2
	14	1083.1
	15	1082.9
	16	1082.8
	17	1082.7
	18	1082.5
Third	19	1082.4
	20	1082.2
	21	1082.0
	22	1081.9
	23	1081.7
	24	1081.6
	25	1081.4
	26	1081.2
	27	1081.0

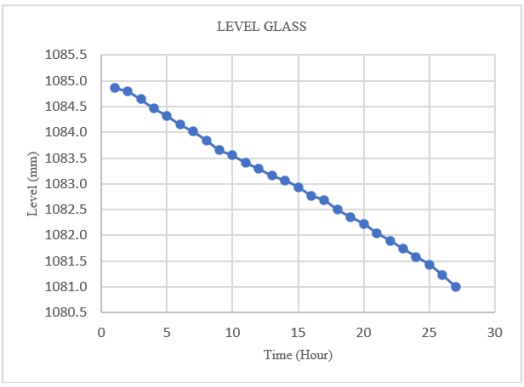

Fig. 13. Decrease in water level in the air circulation variant

Day	Time (Hour)	LEVEL GLASS (mm)
First	1	1084.8
	2	1084.6
	3	1084.4
	4	1084.2
	5	1084.0
	6	1083.8
	7	1083.6
	8	1083.4
	9	1083.1
Second	10	1083.0
	11	1082.8
	12	1082.7
	13	1082.5
	14	1082.2
	15	1082.0
	16	1081.8
	17	1081.5
	18	1081.1
Third	19	1080.9
	20	1080.4
	21	1080.4
	22	1080.4
	23	1080.3
	24	1080.2
	25	1080.0
	26	1079.6
	27	1079.4

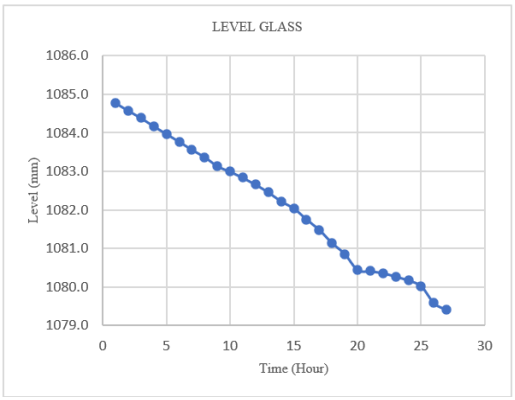

Fig. 14. Decrease in water level in the airtight variant

The calculated saturated vapor pressure of 15.68 kPa exceeds the actual vapor pressure of 12.38 kPa, resulting in a pressure difference of 3.3 kPa that serves as the dominant driving force for mass transfer from the liquid surface to the vapor phase. This phenomenon is reinforced by wind speeds of approximately 22.68 km/h (≈ 6.3 m/s), which, according to empirical formulations, can increase the aerodynamic coefficient from 0.37 to 0.463, representing a relative increase of approximately 25% [49]

Testing in this study was conducted using freshwater because the reactor is still in the trial and initial validation stages of performance. The research focuses on the influence of pressure and temperature on the evaporation rate; therefore, the effects of salt concentration and crystallization have not yet been investigated. The use of seawater at the initial stage may introduce additional phenomena, such as an increase in the boiling point and the formation of salt deposits, which could affect the interpretation of the results. For this reason, salinity or conductivity is not reported in this study and will be examined in subsequent stages of Development.

Table 7 shows that the system's hourly electrical energy consumption is dominated by the centrifugal blower, which consumes 4 kWh, followed by the air heater and the water heater, each consuming 1 kWh. The axial fan consumes 0.75 kWh, while the water pump has the lowest energy demand at 0.125 kWh.

Table 7. Electricity consumption per hour

Unit	Power (Watt)	t (hour)	W (kWh)
Centrifugal blower	4000	1	4
Heater udara	1000	1	1
Heater air	1000	1	1
Water pump	125	1	0.125
Axial fan	750	1	0.75

This pattern indicates that the system's primary energy load originates from the air transfer and heating units, whereas fluid-circulation components have a relatively small impact on total electricity consumption. The contribution of solar heating is not treated as a separate variable because the study is still in the early stages of experimental testing. All experiments were conducted under relatively uniform environmental conditions and time ranges, with the primary heat source being a water heater set to 50–60°C. Quantification and normalization of solar energy contributions are planned for future research using more comprehensive instrumentation.

the comparative analysis between the airtight variant and the air circulation variant indicates that the evaporation rate in the airtight variant configuration is more pronounced. The combination of high fluid temperature, internal circulation, forced airflow, and vacuum conditions [50] influences this condition. These factors act synergistically to maintain uniformity in water-surface temperature while simultaneously enhancing the vapor pressure gradient, which serves as the primary driving force of the mass transfer mechanism [51]. Under the air circulation variant condition, the lack of internal circulation, combined with the open headspace, leads to the Development of temperature stratification within the fluid and an increase in the vapor partial pressure above the liquid surface [52]. This condition decreases the differential between the saturated vapor pressure and the surrounding air (ΔP), thereby yielding a comparatively lower evaporation rate, despite the axial fan's accelerating contribution [53].

The steady-state operating window is determined from the stability of the process parameters in the graph. In the airtight variant (Fig. 15), steady-state conditions are maintained from hour 3 to hour 24 because all parameters, including water temperature, pressure, relative humidity, and airflow velocity, remain stable with minimal fluctuations. In the air circulation variant (Fig. 16), steady-state conditions occur from hours 5 to 24 because the static heating system takes longer to reach thermal equilibrium [54]. This time range is used in the calculation of evaporation, vapor pressure, and theoretical analysis.

Sensitivity analysis shows that headspace conditions strongly influence evaporation performance through changes in partial pressure and relative humidity [55]. A relative variation of ±10% in relative humidity causes a change in the evaporation rate of approximately ±30%, while a change in water temperature of ±5°C results in evaporation rate deviations ranging from −19% to +23%. In contrast, a ±10% change in air velocity produces only a minor effect (<1%). These results confirm that controlling the vapor pressure gradient and maintaining the stability of the water surface temperature are the dominant factors in system performance. In contrast, increasing fan speed has a much smaller influence within the tested operating range.

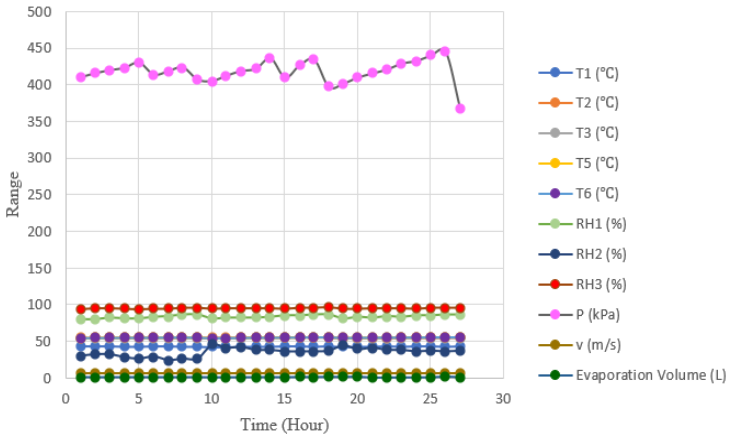

Fig. 15. Full series graph of the airtight variant

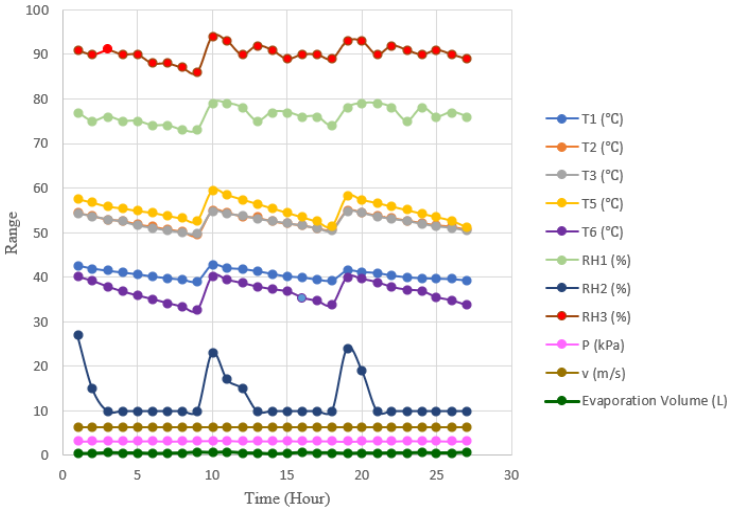

Fig. 16. Full series graph of the air circulation variant

The theoretical separation in this study was carried out by combining the saturated water vapor pressure equation as expressed in Eq. [40], the mass flow rate model due to vapor pressure differences in Eq. [41], and the empirical formulation of the evaporation rate Elp for the air circulation variant as shown in Eq. [45]. By inserting the actual reactor operating conditions, namely water temperature in the range of 50–60°C, an average air flow velocity of 6.3 m/s, and the measured relative humidity values, a saturated water vapor pressure of approximately 15.68 kPa and an actual vapor partial pressure in the headspace of 12.38 kPa were obtained. The difference between these two values yields a driving vapor pressure gradient of approximately 3.3 kPa, which plays a dominant role in the mass transfer mechanism from the liquid phase to the vapor phase.

The parameter sweep analysis was performed using a range of mass transfer coefficient values, with variations in the gas-side mass transfer coefficient within the range of 10^{-3}–10^{-2} m/s, resulting in vapor mass fluxes of 2.07×10^{-5} to 2.07×10^{-4} kg·m^{-2}·s^{-1}, which are equivalent to an evaporation rate of approximately 1.79 L·m^{-2}·day^{-1}. The maximum predicted value approaches the experimental results when the gas-side mass transfer coefficient is at the upper limit of this range. Further sensitivity analysis indicates that changes in the vapor pressure difference have the most significant effect: a 10% increase in the pressure difference increases the evaporation rate by approximately 8–9%, whereas variations in air velocity within the range of 3–8 m/s have only a relatively small effect.

During test implementation, the system was operated using non-saline raw water as the initial test medium rather than seawater. Therefore, scale formation due to salt precipitation has not yet become a dominant factor in this experiment (Fig. 17). Nevertheless, the possibility of dirt or scale accumulation was anticipated by performing manual cleaning between each test to maintain consistent conditions on the heating surface and reactor walls. From a continuous operation perspective, the use of seawater at a later stage is expected to increase the risk of scale formation, potentially reducing heat and mass transfer efficiency. Accordingly, implementing the system under high-salinity conditions will require periodic maintenance strategies and more comprehensive scale mitigation measures to ensure long-term performance stability.

Fig. 17. Salt container

Accordingly, the system configuration in the airtight variant exhibits superior performance, supported by both experimental results and the theoretical framework for heat- and mass-transfer mechanisms and fluid behavior in a confined thermal environment. Such effectiveness indicates the successful integration of low-pressure principles, active fluid circulation, and airflow utilization to facilitate a more intensive and efficient evaporation process [56].

4 Conclusions

This study analyzes the effects of pressure and water temperature on evaporation performance in an 8000 L-capacity desalination reactor, comparing air-circulation and airtight configurations. Under comparable operating conditions (50–60 °C and ±6.3 m/s), the airtight configuration produced an evaporation volume of 20.12 L over 27 hours, 16.64% higher than the air-circulation configuration, which produced 17.25 L. This improvement is attributed to the formation of a partial vacuum, which reduces internal pressure and increases the vapor pressure gradient, and to active hot-water circulation, which maintains temperature uniformity and enhances mass-transfer effectiveness. The experimental results for the airtight configuration also exceeded theoretical estimates by 15.5%, indicating a synergy between low pressure, fluid flow, and forced air flow. Overall, these findings confirm that integrating an airtight system with active circulation is a practical approach to improving evaporation performance in large-scale thermal desalination systems.

Acknowledgment

Thank you to the Directorate of Research, Technology, and Development (DRTPM), Ministry of Education, Culture, Research, and Technology (Kemdikbudristek), for research and community service support under Decree Number 0667/E5/AL.04/2024 and Agreement/Contract Number 812/LL3/AL.04/2024 (094/F.03.07/2024), as well as to the Faculty of Industrial Technology and Informatics, UHAMKA, for the support, guidance, and financial assistance provided, which enabled this research to be carried out correctly and to achieve the expected results. This support not only facilitated the smooth implementation of the research process but also served as a significant source of motivation for the author in completing this scientific work.

References

[1] UNESCO, "Valuing water," United Nations Educational, Scientific and Cultural Organization, 2021.

[2] W. Musie and G. Gonfa, "Fresh water resource, scarcity, water salinity challenges and possible remedies: A review," Aug. 01, 2023, *Elsevier Ltd*. doi: 10.1016/j.heliyon. 2023. e18685.

[3] F. Ali, D. L. Lestari, M. D. Putri, and K. N. Azmi, "Strategy Analysis for the Fulfilment of Clean Water Needs Through Piped-Water Service in Metropolitan City during the COVID-19 Pandemic," *International Journal of Technology*, vol. 15, no. 5, pp. 1237–1246, 2024, doi: 10.14716/ijtech.v15i5.6160.

[4] Y. Agnesia and J. Fitri, "Perubahan iklim dan dampaknya pada kesehatan lingkungan," Jul. 2025.

[5] WHO and UNICEF, "Progress on household drinking water, sanitation and hygiene," 2024.

[6] A. W. Krisdiarto, A. Ferhat, M. Prasanto Bimantio, I. P. Stiper, and Y. Jl, "penyediaan air bagi masyarakat pesisir terdampak kekeringan dengan teknologi desalinasi air laut sederhana," 2020.

[7] Z. Zhong, M. Burhan, K. C. Ng, X. Cui, and Q. Chen, "Low-temperature desalination driven by waste heat of nuclear power plants: A thermo-economic analysis," *Desalination*, vol. 576, May 2024, doi: 10.1016/j.desal.2024.117325.

[8] D. Dicky Yhavez, M. Meddy Danial, and dan Arfena Deah Lestari, "Desalinasi air laut menggunakan metode reverse osmosis (RO) dengan variasi tekanan pompa," 2024.

[9] A. M. Yusuf, D. Mugisidi, I. P. Aji, and O. Heriyani, "Pengaruh vakum pada penguapan air laut," *Rekayasa Energi Manufaktur) Jurnal* |, vol. 8, no. 2, pp. 2528–3723, 2023, doi: 10.21070/rem.v8i2.1672.

[10] A. Alenezi and Y. Alabaiadly, "Emerging technologies in water desalination: A review and future outlook," Mar. 01, 2025, *Elsevier Ltd*. doi: 10.1016/j.nexus.2025.100373.

[11] A. Rifai *et al.*, "pengaruh tekanan pada reverse osmosis terhadap penyisihan kadar ion klorida (Cl-) dan total dissolved solids (TDS) pada pengolahan air payau," vol. 25, no. 2, pp. 300–307, Jul. 2024.

[12] S. H. Aladwani, M. A. Al-Obaidi, and I. M. Mujtaba, "Performance of reverse osmosis-based desalination process using spiral wound membrane: Sensitivity study of operating parameters under variable seawater conditions," *Clean Eng Technol*, vol. 5, Dec. 2021, doi: 10.1016/j.clet.2021.100284.

[13] M. R. Qtaishat *et al.*, "Desalination at ambient temperature and pressure by a novel class of biporous anisotropic membrane," *Sci Rep*, vol. 12, no. 1, Dec. 2022, doi: 10.1038/s41598-022-17876-8.

[14] S. Winarni and Syahrial, "Air dan miskonsepsinya: Suatu tinjauan ilmu kimia," Aug. 2020.

[15] Ismiyati and F. Sari, "Identifkasi kenaikan titik didih pada proses evaporasi, terhadap konsentrasi larutan sari jahe," Oct. 2020.

[16] S. Kumar, S. S. Salins, H. K. Sachidananda, K. Prasad, and S. V. K. Reddy, "Effect of air flow rate and operating time on the evaporator performance of solar air conditioning system," *Discover Applied Sciences*, vol. 7, no. 4, Apr. 2025, doi: 10.1007/s42452-025-06652-8.

[17] A. Sutrisno, Mirmanto, and Syahrul, "Pengaruh kecepatan udara terhadap kinerja mesin air water harvester dengan dua evaporator koil," Nov. 2023.

[18] R. Omar, C. P. Zanutto, S. Ambrose, D. Hann, and C. Eastwick, "Experimental and analytical investigation on the evaporation characteristics of single and binary component droplets in a hot air stream," *Appl Therm Eng*, vol. 278, Nov. 2025, doi: 10.1016/j.applthermaleng.2025.126993.

[19] M. Irham, H. Frans Sangian, M. Daurina Bobanto Jurusan Fisika, and F. Matematika dan Ilmu Pengetahuan Alam Universitas Sam Ratulangi, "Desain dan konstruksi alat desalinasi air laut dengan menggunakan metode destilasi konvektif dipaksakan," 2024.

[20] Alamsyach Rizky, "Laju penguapan pada forced flow solar still," 2024.

[21] N. Ghazouani, A. A. El-Bary, G. E. Hassan, N. Becheikh, A. Bawadekji, and M. M. Elewa, "solar desalination by humidification–dehumidification: A review," Nov. 01, 2022, *MDPI*. doi: 10.3390/w14213424.

[22] G. Konapala, A. K. Mishra, Y. Wada, and M. E. Mann, "Climate change will affect global water availability through compounding changes in seasonal precipitation and evaporation," *Nat Commun*, vol. 11, no. 1, Dec. 2020, doi: 10.1038/s41467-020-16757-w.

[23] Z. Mardoni, "Analysis of salt production, consumption and import in Indonesia," 2022. [Online]. Available: http://ijsoc.goacademica.com

[24] M. A. Munir, R. A. Rahman, and D. D. Rahmalina, "Pengembangan alat desalinasi air laut dengan teknologi thermal energy storage development of seawater desalination equipment with technology thermal energy storage," vol. 5, pp. 170–178, 2023.

[25] R. Natawisastra, R. Bramawanto, M. ' Muri, L. Alfaris, and & Suhernalis, "Rancang bangun alat destilasi air laut yang dilengkapi pemanas air sederhana," Jul. 2022.

[26] I. W. Joniarta, A. Aprilian Dika, and M. Wijana, "Analisis efisiensi pompa sentrifugal pada desalinasi dengan proses reverse osmosis," *Energy, Materials and Product Design*, vol. 3, no. 2, pp. 213–223, Nov. 2024, doi: 10.29303/empd.v3i2.5429.

[27] Nurdin, Murhaban, and H. Darsan, "Analisis pengaruh beban terhadap kinerja induced draft fan pada siklus udara gas buang," Sep. 2022.

[28] Nurkholid, D. Mugisidi, Widodo, O. Heriyani, and I. Sulistiono, "Enhancing Seawater desalination performance using a vortex generator in a modified window air conditioner," *Disseminating Information on the Research of Mechanical Engineering-Jurnal Polimesin*, vol. 23, no. 1, Feb. 2025, [Online]. Available: http://e-jurnal.pnl.ac.id/polimesin

[29] S. Febriani, "Analisis deskriptif standar deviasi," 2022.

[30] Nurhaswinda *et al.*, "Ukuran dispersi," Apr. 2025.

[31] F. Isnomo Abdi, D. Wulandari, and D. Puspitasari, "Inovasi kompor berbahan bakar oli bekas menggunakan tekanan uap air," Apr. 2024, [Online]. Available: https://ejournal.unesa.ac.id/index.php/jurnal-rekayasa-mesin

[32] T. Ibotov *et al.*, "Finding the acceleration due to gravity using the hydrostatic pressure simulation of PhET," *Indonesian Journal of Innovation and Applied Sciences (IJIAS)*, vol. 5, no. 1, pp. 26–32, Feb. 2025, doi: 10.47540/ijias.v5i1.1742.

[33] W. Gunawan, A. Dyah Juniarti, and D. Rosihan, "Audit energi listrik pada bangunan gedung kampus 1 universitas bantan jaya (studi kasus gedung 4 universitas banten jaya)," *Jurnal InTent*, vol. 5, no. 2, 2022.

[34] A. Somalinggi, S. Tongkukut, and H. F. Sangian, "Analisis air hasil desalinasi menggunakan metode distilasi konvektif dipaksakan," *Jurnal LPPM Bidang Sains dan Teknologi*, vol. 8, no. 2, pp. 85–91, Oct. 2023.

[35] X. Luo, J. Shi, C. Zhao, Z. Luo, X. Gu, and H. Bao, "The energy efficiency of interfacial solar desalination: insights from detailed theoretical analysis," 2023.

[36] D. Khalid Ahmed and R. Ahmed Mahmood, "The evaporation process in a heat pipe: A review study," 2025, [Online]. Available: www.techniumscience.com

[37] W. S. Damanik, M. A. Siregar, S. Lubis, and Siregar. Ahmad M, "Kajian pengaruh ketebalan kaca evaporator terhadap energi yang diserap kolektor pada proses desalinasi air laut," *Jurnal Rekayasa Material, Manufaktur dan Energi*, vol. 4, no. 2, Sep. 2021, doi: 10.30596/rmme.v4i2.8071.

[38] H. Riupassa, H. H. Taba, and I. Kolago, "Analisa perpindahan panas pada pemanas air tenaga surya dengan variasi diameter pipa bentuk sinusoidal," Dec. 2020.

[39] S. N. Razali, A. Ibrahim, A. Fazlizan, A. B. Al-Aasam, M. A. A. Rahmat, and M. A. A. Bin Ishak, "Superior thermal dissipation through natural convection in a passive cooling system using multidirectional tapered fin heat sinks (MTFHS)," *International Journal of Renewable Energy Development*, vol. 14, no. 3, pp. 577–587, May 2025, doi: 10.61435/ijred.2025.60742.

[40] I. Sulistiono, D. Mugisidi, Nurkholid, and Oktarina Heriyani, "Effect of wind speed on evaporation rate in air conditioner based desalination units," *TEKNOSAINS : Jurnal Sains, Teknologi dan Informatika*, vol. 12, no. 1, pp. 54–61, Jan. 2025, doi: 10.37373/tekno.v12i1.1238.

[41] R. Wirangga, D. Mugisidi, A. T. Sayuti, and O. Heriyani, "The impact of wind speed on the rate of water evaporation in a desalination chamber," *Journal of Advanced Research in Fluid Mechanics and Thermal Sciences*, vol. 106, no. 1, pp. 39–50, Jun. 2023, doi: 10.37934/arfmts.106.1.3950.

[42] M. Uddin *et al.*, "Design a cooling pillow to support a high-speed supercritical CO2 turbine shaft," *Appl Therm Eng*, vol. 196, Sep. 2021, doi: 10.1016/j.applthermaleng.2021.117345.

[43] T. Poós and E. Varju, "Review for convection based evaporation of open liquid surface and equations of evaporation rate," *International Communications in Heat and Mass Transfer*, vol. 157, Sep. 2024, doi: 10.1016/j.icheatmasstransfer.2024.107755.

[44] H. W. Fung, M. A. Mahmud, and B. D. MacDonald, "Experimental investigation of forced convection on evaporation of continuously-fed sessile droplets," *International Journal of Thermal Sciences*, vol. 175, May 2022, doi: 10.1016/j.ijthermalsci.2022.107459.

[45] G. Indah Budiarti and M. Shinta Amelia, *Operasi Perpindahan Massa dan Panas*. 2022.

[46] S. M. Habib, A. Hamed, A. Y. Youssef, M. Kassem, and A. Hanafi, "dynamic modeling and simulation of the forward feed MED-TVC desalination plant," *Journal of Advanced Research in Fluid Mechanics and Thermal Sciences*, vol. 92, no. 1, pp. 190–211, 2022, doi: 10.37934/arfmts.92.1.190211.

[47] F. Aguirre Correa, J. V. G. DE ARELLANO, R. Ronda, F. Lobos-Roco, F. Suárez, and O. Hartogensis, "evaporation driven by atmospheric boundary layer processes over a shallow saltwater lagoon in the altiplano," *J Hydrometeorol*, vol. 25, no. 8, pp. 1113–1134, Aug. 2024, doi: 10.1175/JHM-D-23-0105.1.

[48] M. L. Roderick, C. Jayarathne, A. J. Rummery, and C. J. Shakespeare, "Evaluation of a wind tunnel designed to investigate the response of evaporation to changes in the incoming long-wave radiation at a water surface," *Atmos Meas Tech*, vol. 16, no. 20, pp. 4833–4859, Oct. 2023, doi: 10.5194/amt-16-4833-2023.

[49] S. Guseva *et al.*, "Bulk transfer coefficients estimated from eddy-covariance measurements over lakes and reservoirs," *Journal of Geophysical Research: Atmospheres*, vol. 128, no. 2, Jan. 2023, doi: 10.1029/2022JD037219.

[50] O. Khan, S. Mufazzal, Z. A. Khan, A. F. Sherwani, Z. Yahya, and A. Alhodaib, "Optimizing the performance parameters of vacuum evaporation technology for management of anaerobic digestate in a waste water treatment plant using fuzzy MCDM method," *Desalination Water Treat*, vol. 320, Oct. 2024, doi: 10.1016/j.dwt.2024.100864.

[51] G. Wang, Z. Zhang, T. Jiang, J. Lin, and Z. Chen, "Thermodynamic and optical analyses of a novel solar CPVT system based on parabolic trough concentrator and nanofluid spectral filter," *Case Studies in Thermal Engineering*, vol. 33, May 2022, doi: 10.1016/j.csite.2022.101948.

[52] D. Mugisidi, A. Fajar, Rifky, and O. Heriyani, "Peningkatan efisiensi dan efektivitas kondensor pada solar still increasing the efficiency and effectiveness of the condensor on the solar still," Dec. 2022.

[53] F. T. Jodah, W. H. Alawee, H. A. Dhahad, and Z. M. Omara, "Improving the productivity of a spherical solar still with an axial absorber plate through multiple enhancements," *Results in Engineering*, vol. 28, Dec. 2025, doi: 10.1016/j.rineng.2025.107217.

[54] D. Haryanto, A. Budiman, M. Putra, P. Setiawan, and M. Juarsa, "Komisioning pemanas listrik pada heating tank section helical pipe heat exchanger," *DISTILAT: Jurnal Teknologi Separasi*, vol. 10, no. 1, pp. 160–169, Mar. 2024, doi: 10.33795/distilat.v10i1.3936.

[55] Y. L. Jiang, J. R. Ruiz, R. Friend, and J. P. Reid, "Characterizing the influence of relative humidity and ethanol content on the dynamic size distributions of aerosols generated from a soft mist inhaler," *Pharm Res*, vol. 42, no. 4, pp. 651–663, Apr. 2025, doi: 10.1007/s11095-025-03851-1.

[56] A. Prasad, "A Review on Evaporation," *International Journal of Pharmaceutical Research and Applications*, vol. 7, p. 273, Mar. 2022, doi: 10.35629/7781-0702273285.